Journal of Analysis and Testing (2023) 7:260–271
https://doi.org/10.1007/s41664-023-00256-0

REVIEW

Emerging NIR-II Luminescent Gold Nanoclusters for In Vivo Bioimaging

Siqi Ni[1] · Yizhuo Liu[1] · Shufen Tong[1] · Shihua Li[1] · Xiaorong Song[1,2]

Received: 26 May 2023 / Accepted: 30 June 2023 / Published online: 14 August 2023

Abstract
Gold nanoclusters (AuNCs) with near-infrared II (NIR-II) photoluminescence (PL) have emerged as novel bioimaging probes for in vivo disease diagnosis. So far, it still lacks a systematic review focusing on the synthesis, PL tuning, and in vivo imaging of NIR-II luminescent AuNCs. In this review, we briefly introduce the synthesis of NIR-II luminescent AuNCs using various surface ligands. We discuss the origins and properties of NIR-II PL in AuNCs, and summarize the strategies for improving and/or tuning NIR-II PL emissions. We also provide an overview of the recent progress in the application of AuNCs in tumor-targeted imaging, molecular imaging, and other areas (such as the sensitive imaging of bones, vessels, lymph nodes, etc.). Finally, we present the prospects and challenges in the field of NIR-II luminescent AuNCs and related imaging applications, expecting to offer comprehensive understanding of this field, and thereby deepening and broadening the biological application of AuNCs.

Keywords Gold nanoclusters · NIR-II · Fluorescent probe · In vivo imaging · Bioimaging

1 Introduction

Gold nanoclusters (AuNCs) with typical ultrasmall size of 1–3 nm, as an emerging kind of bioimaging and therapeutic agents, have aroused increasing attentions in the biomedical fields [1–6]. In general, gold is considered as a biocompatible element. Since the pioneer tried to utilize [$KAu(CN)_2$] as an anti-bacteria drug in 1890, the past few decades have witnessed rapid development of gold-based therapeutic drugs for diverse diseases, including arthritis, psoriasis, and tumors [7–9]. For example, thiolated Au(I) complexes such as sodium aurothiomalate (Myocrisin™) are widely used to treat rheumatoid arthritis in clinics. Despite such achievements, Au(I) complexes may inhibit reductase activity and the mitochondrial function of thioredoxin, causing some potential toxicities [10–12]. It, thus, remains a big challenge to improve the therapeutic effect of gold-based complexes and lower their toxicity, which makes them less attractive than platinum-based drugs [13]. In this regard, the research upsurge of AuNCs may open a new avenue to engineer gold for clinical biomedical applications.

In comparison with the large-size gold nanoparticles (NPs, > 3 nm), AuNCs showed some unique physicochemical attributes, especially the definable structures, discrete electronic states, and photoluminescence (PL) properties [14–17]. Luminescent AuNCs have nowadays shown great promise for biomedical application, ranging from in vitro biosensing to in vivo bioimaging [18–22]. This motivates the exploration of new strategies to improve the PL quantum yield of AuNCs and the discovery of new PL performance, along with the increasing understanding of PL mechanisms and other functions (Fig. 1) [23–30]. In particular, NIR-II luminescent AuNCs (i.e., 1000–1700 nm) have attracted much interest in recent years, enabling better in vivo imaging sensitivity and resolution than that of traditional AuNCs with visible and NIR-I emission (i.e., 400–800 nm) [31–33]. Recently, atomically precise NIR-II AuNCs can be elegantly synthesized and tailored for diverse in vivo bioimaging applications, such as blood vessel imaging,

✉ Shihua Li
lishihua@126.com

✉ Xiaorong Song
xrsong@fzu.edu.cn

[1] MOE Key Laboratory for Analytical Science of Food Safety and Biology, Engineering Technology Research Center on Reagent and Instrument for Rapid Detection of Product Quality and Food Safety in Fujian Province, College of Chemistry, Fuzhou University, Fuzhou 350108, China

[2] Fujian Science & Technology Innovation Laboratory for Optoelectronic Information of China, Fuzhou 350108, China

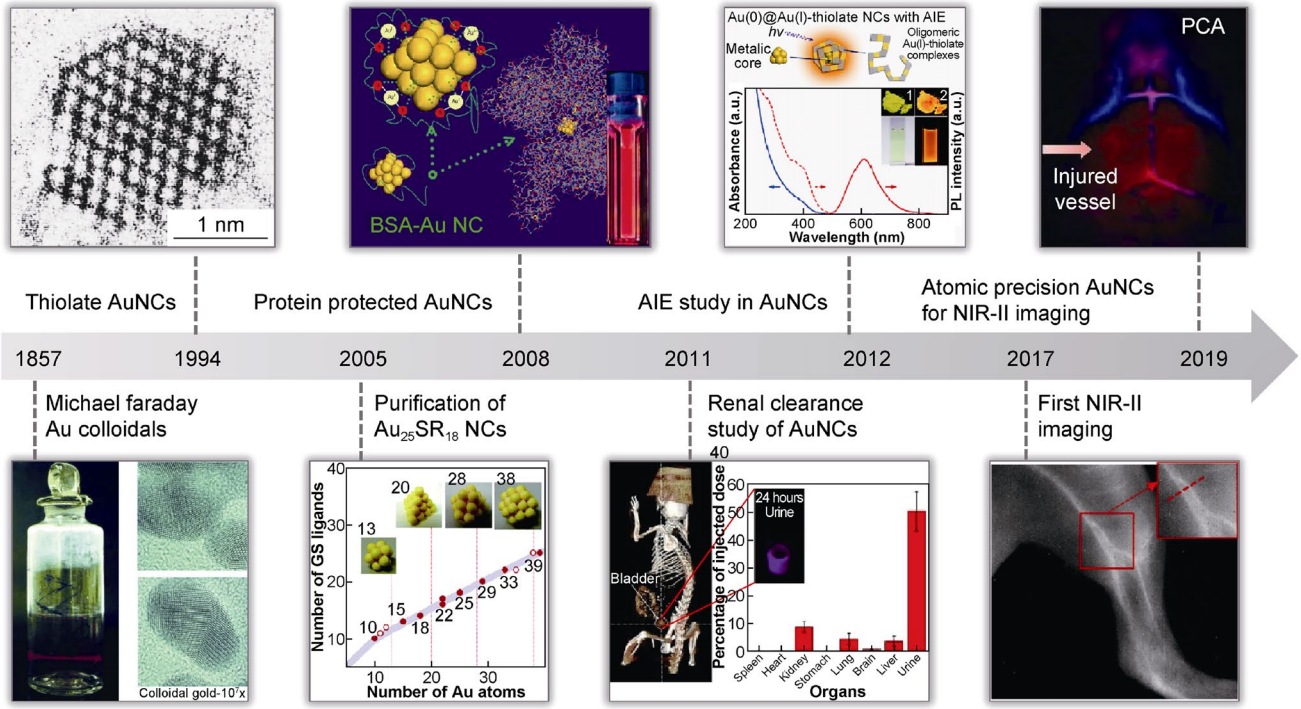

Fig. 1 Timeline of some significant events in the synthesis, properties and bioimaging of AuNCs. Reproduced with permission from Ref. [23–30]. Copyright Wiley–VCH, American Chemical Society

molecular imaging, and disease-targeted specific imaging [34–36]. Together with good renal clearance and computed tomography(CT) imaging capabilities, NIR-II luminescent AuNCs are anticipated to provide promising tools for practical in vivo sensitive and multifunctional bioimaging in the future [26, 37, 38].

Despite such exciting advances, the research on NIR-II luminescent AuNCs is just on its infancy and there are also some challenges in this field. Currently, it still lacks a systematic review focusing on the synthesis, PL tuning, and in vivo bioimaging of NIR-II luminescent AuNCs. In this review, we first briefly introduced the synthesis of NIR-II luminescent AuNCs using different surface ligands. Then, the NIR-II PL origins and properties of AuNCs were discussed, along with summarizing the strategies to improve and/or tune the NIR-II PL emissions. We subsequently detailed the recent progress on the application of AuNCs in tumor-specific bioimaging and others (such as the sensitive imaging of bones, vessels, lymph nodes, etc.). Finally, we presented the prospects and challenges in NIR-II luminescent AuNCs and related imaging applications, expecting to offer comprehensive understanding of this field, and thereby deepening and broadening the biological application of AuNCs.

2 Synthesis of NIR-II Luminescent AuNCs

In fact, most of NIR-II luminescent AuNCs have been previously synthesized, albeit a few exceptions. In 2019, Xie and Zhang reported the NIR-II PL in glutathione (GSH)-protected Au_{25}NCs emitting at 1100–1350 nm [23]. The synthesis of this GSH-Au_{25}NCs was conducted by using CO as reductant under alkaline condition, which was previously established by Xie's group [39]. In addition, Xie et al. synthesized the NIR-II emitting $Au_{44}MBA_{26}$ NCs (MBA denotes 4-mercaptobenzoic acid) via NaOH-mediated $NaBH_4$ reduction method, and the Au_{44}NCs displayed two PL emission peaks centered at ~ 1080 nm and ~ 1280 nm when excited at 808 nm [40]. Motivated by this, several ligands have been attempted to synthesize NIR-II luminescent AuNCs under similar conditions using monothiol, dithiol, and pegylated thiol ligands [35, 36]. For example, we utilized a macromolecular ligand (i.e., thiolated cyclodextrin, CDS) as the surface protective agent and synthesized NIR-II-emitting CDS-AuNCs with PL at around 1050 nm [35]. To improve the NIR-II PL efficacy or tune biofate, dual or multiple ligands have recently been employed synergistically in the synthesis of NIR-II luminescent AuNCs, in which the thiolated Au(I)

complexes are first formed, followed by the reduction of sodium borohydride at certain stoichiometric ratios [36, 41].

Besides, proteins (e.g., bovine serum albumin, BSA) have been utilized as template to synthesize NIR-II AuNCs [42–45]. Unlike the synthesis of NIR-I-emitting BSA-AuNCs using BSA as protective agent and reductant simultaneously, it needs to add additional reductants such as sodium borohydride in the reaction system. It is worthy to mention that, BSA-AuNCs not only enable improved stability and blood circulation performance than that protected by small thiolated ligands, but also may confer them with multiple functional groups for further application. For example, ribonuclease-A (RNase-A) protein with rich species of amino acids has been exploited as template to synthesize highly NIR-II luminescent AuNCs, meanwhile allowing for good stability and biocompatibility in the gastrointestinal tract [42]. Xiao et al. also synthesized NIR-II luminescent BSA-AuNCs and conjugated them with Gd-complexes for dual-modal bioimaging and photodynamic therapy [43]. Therefore, the synthesis of NIR-II AuNCs has no many differences from the traditional protocols of AuNCs and can be adapted rationally according to particular protective agents and application requirements. But, it should be noted that the developed atomically precise AuNCs did not include many species, such as Au_{25}, Au_{44}, Au_{11}, and Au_{23}, which emphasized the need of future increasing exploration on NIR-II luminescent AuNCs [46, 47].

3 Properties and Regulation Strategies of NIR-II PL

Understanding the origins (or mechanisms) of PL is highly important to explore new effective NIR-II luminescent AuNCs. However, so far, there are only few reports addressing this aspect [48, 49]. Interestingly, atomically precise Au_{25}NCs with both visible and NIR-II PL are among the best candidates for studying PL origins correlating to structures. Zhou et al. systematically studied the origins of visible and NIR-II PL in the $Au_{25}(SR)_{18}$ NCs through experimental characterizations and theoretical calculations [49]. Specially, by examining Au_{25}NCs with different surface ligands, the researchers found that the NIR-II and visible PL in $Au_{25}(SR)_{18}$ AuNCs likely originate from the Au_{13} core state and core-surface charge transfer state, respectively. NIR-II PL can be enhanced by increasing the rigidity of surface ligands, and exhibits single- or double-exponential lifetime decays obeying the energy gap law. In an effort to reveal the fundamental electronic transitions in NIR-II luminescent AuNCs, Li et al. investigated the NIR-II PL properties of rod-shaped bi-icosahedral Au_{25}NCs caped with triphenylphosphine and 2-phenylethanethiol ligands [48]. Notably, the rod Au_{25}NCs showed NIR-II PL centered at around 1520 nm with a high PL quantum yield of approximately 8%, which was rarely observed in other AuNCs. The authors proved the great significance of the central Au atom in enhancing the NIR-II PL by suppressing the non-radiative transition, as corroborated by the density functional theory (DFT) calculations. This revealed the underlying origin of NIR-II PL and highlighted the vital role of atomic engineering in improving the NIR-II PL of AuNCs.

Many researches have been devoted to enhancing and tuning the emission of NIR-II luminescent AuNCs, which, however, is a tough task. This is because of the different underlying electronic transitions compared to traditional visible luminescent AuNCs, of which there are several available strategies to improve their PL quantum yields, such as atom doping, aggregation-induced emission effect and surface rigidification [25, 50, 51]. Currently, NIR-II PL of AuNCs can generally be enhanced using two main strategies, including atom doping and ligand engineering. The latter strategy can be achieved by regulating ligand properties, surface rigidification, and ligand exchange reactions (Fig. 2). Zhang et al. studied the single-atom doping effect on the NIR-II PL of Au_{25}NCs, by doping various atoms such as Zn, Cd, Cu, Ag, and Pt (Fig. 3a) [52]. It was found that the majority of atom doping treatments can enhance NIR-II PL, and $Au_{25}Cd_1$NCs exhibited the

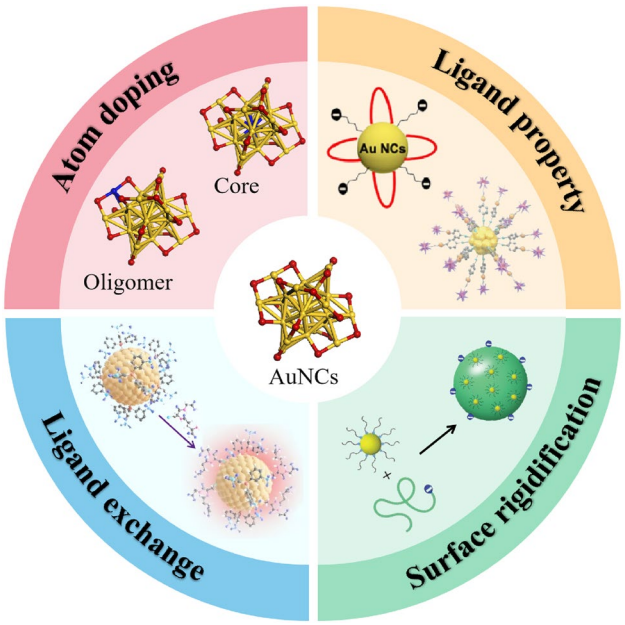

Fig. 2 Schematic illustration of the NIR-II PL regulation strategies of AuNCs. The NIR-II PL of AuNCs could be enhanced by doping atoms in the core or surface motifs, imparting suitable ligands (e.g., dithiol ligands), and encapsulating in the matrix (e.g., BSA). Reproduced with permission from Ref. [36, 40, 53, 54]. Copyright Wiley–VCH, American Chemical Society, Royal Society of Chemistry

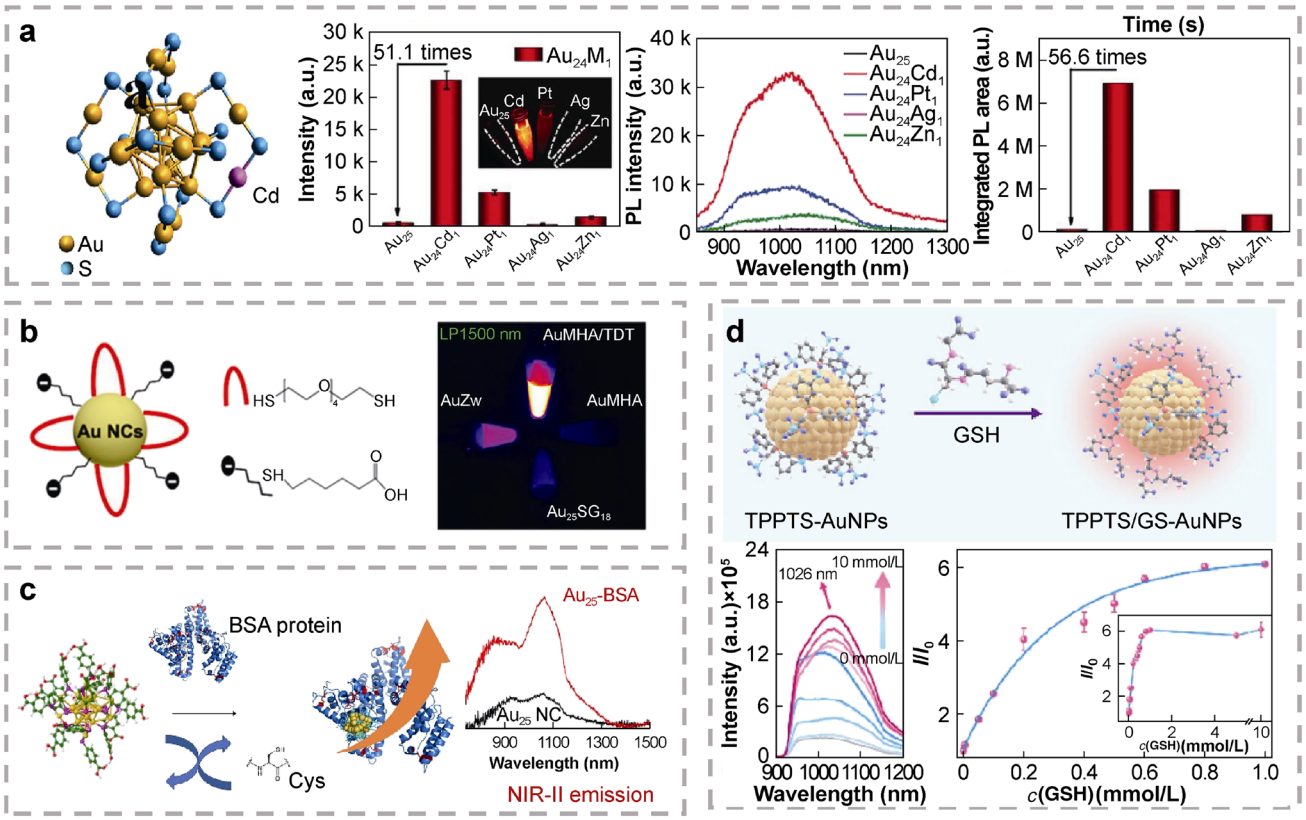

Fig. 3 Regulation of NIR-II PL in AuNCs. **a** Structure of $Au_{24}Cd_1$NCs and NIR-II PL images, spectra and integrated PL area of Cd-, Pt-, Ag-, and Zn-doped Au_{25}NCs, under an excitation of 808 nm. Reproduced with permission from Ref. [52]. Copyright 2023, Wiley–VCH; **b** Scheme illustration of the structure and NIR-II PL of AuNCs protected by mercaptohexanoic acid (MHA)/tetra (ethylene glycol) dithiol (TDT), MHA, GSH, and etc. Reproduced with permission from Ref. [36]. Copyright 2020, American Chemical Society; **c** Scheme illustration of the incorporation of Au_{25}NCs into BSA and corresponding PL spectra (λ_{ex} = 700 nm). Reproduced with permission from Ref. [55]. Copyright 2022, Elsevier; **d** Schematic illustration of ligand exchange process of TPPTS-AuNCs by GSH, and the PL spectra and intensity changes at different GSH concentrations. Reproduced with permission from Ref. [53]. Copyright 2022, American Chemical Society

highest NIR-II PL intensity, enabling about 56-fold higher than Au_{25}NCs. The electronic and optical properties of the Cd-doped Au_{25}NCs were studied by DFT. The results suggested that the increased electron donation from the Cd to Au on the surface could create a new energy level, which may, thus, decrease the HOMO–LUMO gap and lead to the PL enhancement.

Regarding the ligand engineering strategy, it is achievable to choose suitable thiolated ligand to synthesize NIR-II luminescent AuNCs and improve the PL performance. For example, Guével et al. found that the utilization of bidentate dithiol ligands could largely increase the NIR-II PL of AuNCs, which also imparted the AuNCs with anisotropic charges that may lead to the red-shift of PL and the self-assembly of AuNCs (Fig. 3b) [36]. The group further observed effective PL enhancement (about 4.7-fold) of NIR-II luminescent AuNCs after the post-synthesis incorporation of thiolated Au_{25}NCs into BSA protein, together with the prolonged PL lifetime from 72.1 ns to 936.1 ns (Fig. 3c) [55]. Such NIR-II PL enhancement could be attributed to the surface rigidification-reinforced intersystem crossing and the contribution of core–shell charge transfer states. In addition, Liu's group recently demonstrated a ligand exchange way to improve the NIR-II PL of AuNCs (Fig. 3d) [53]. In this work, the poorly luminescent AuNCs protected by the triphenylphosphine-3,3′,3″-trisulfonic acid (TPPTS) ligands were primarily synthesized and could further be activated with GSH for boosting NIR-II PL, due to the enhanced ligand-to-metal charge transition effect. Considering the fact that current NIR-II PL quantum yields in the hydrophilic AuNCs are frequently very low (e.g., < 1%), it is still extremely demanded to explore effective strategies to design high NIR-II luminescent AuNCs for bioapplications.

4 Bioimaging Applications of In Vivo NIR-II PL

The emerging NIR-II PL has promoted bioimaging application of AuNCs nanoprobes into a new realm of imaging resolution and sensitivity [31–33]. In the past five years, NIR-II luminescent AuNCs were carefully designed as biolabels and nanoprobes for in vivo bioimaging. In this section, we will summarize and discuss the design strategies and imaging performances of NIR-II luminescent AuNCs in tumor imaging, biomarker imaging, and others (e.g., the imaging of kidney injury and blood vessels).

4.1 Tumor Imaging

Tumor is still one of the biggest challenges in the biomedical field, necessitating the development of sensitive diagnosis techniques [56–58]. Nowadays PL imaging as a nondestructive and sensitive imaging model has drawn increasing interest [59–61]. To apply AuNCs for in vivo tumor imaging, AuNCs are often engineered with proteins or antibodies to capacitate relatively long blood circulation time. For example, RNase-A-capped AuNCs have been implemented to visualize the gastrointestinal tract and also diagnose intestinal tumors, which cannot be achieved by leveraging quantum dots and lanthanide NPs due to their low stability in the acidity condition of the gastrointestinal tract (Fig. 4a) [42]. The AuNCs can achieve the sensitive and high-resolution NIR-II PL imaging of intestinal tumors of size down to 2.5 mm, presenting their good imaging capability in harsh biological environment. To realize tumor-specific imaging, we developed a new class of NIR-II luminescent AuNCs protected by thiolated CD ligands that enabled facile conjugation to antibodies through the robust host–guest interaction between CDS and adamantane (Fig. 4b) [35]. This strategy could successfully label anti-CD326 antibody with CDS-AuNCs for the sensitive tumor-targeted NIR-II PL imaging.

NIR-II luminescent AuNCs can also be implemented for tracking tumor metastasis. Noteworthy, tumor metastasis is the leading cause of the death of tumor patients, and the sentinel lymph nodes are the first metastasis places [62–65]. It is, thus, an urgent need to realize the specific imaging of sentinel lymph nodes for evaluating tumor metastasis status and guiding surgical excision [66, 67]. Jiang et al. engineered AuNCs with the rational surface coating of dual or multiple ligands, which can impart them with suitable charge density and biostability for improving lymph node targeting capability (Fig. 5a) [41]. This AuNCs nanoprobe not only enabled the long-term tracking and surgical navigation of lymph nodes, but also can be incorporated with chemotherapeutic drugs for the therapy of metastatic tumors in lymph nodes without causing hepatotoxicity. In recent years, the researchers have also devoted to a consistent pursuit of improving the targeting efficacy to certain disease tissues. To reduce the unspecific accumulation of AuNCs in the bones, Dai's group lately developed an interesting strategy by modifying GSH-AuNCs with 4-aminophenylphosphorylcholine (PC in short), which was found to effectively bypass their bone accumulation and augment lymph node targeting effect (Fig. 5b) [68]. Facilitated by the rapid renal clearance (up to about 100% at 24 h post injection), PC-modified AuNCs can be applied to sensitive NIR-II PL imaging of lymph nodes and the metastatic tumors with high signal-to-noise ratio, outperforming than GSH-AuNCs and the clinical used indocyanine green.

4.2 Molecular Imaging of Biomarkers

Molecular imaging is a booming research discipline that aims at achieving specific analysis of molecular targets associated with the occurrence and progression of diseases [69–71]. It is particularly helpful to the personalized diagnosis and treatment of diseases. In this application scenario, the inherent responsiveness of AuNCs to target molecules such as reactive oxygen species (ROS) and hydrogen sulfide (H_2S) can be utilized for specific molecular imaging in vivo [72–76]. We recently developed a smart nanoprobe based on the core-satellite assemblies of NIR-II luminescent AuNCs and lanthanide NPs, which emitted at 1100 nm and 1550 nm, respectively (Fig. 6a) [34]. The NIR-II PL of AuNCs can be quenched by H_2S, while the NIR-II PL of lanthanide NPs kept unchanged, thus realizing in vivo ratiometric NIR-II PL imaging of H_2S in mice liver. The sensing mechanism of AuNCs towards H_2S was found to be related with the high reducibility of H_2S, which reduces Au(I) species and destroy AuNCs' structure. These nanoprobes enabled sensitive in vitro H_2S detection and in vivo delivery efficacy evaluation of the H_2S-prodrugs in the liver. Similarly, Zhang et al. constructed the nanoassemblies based on AuNCs and down-/up-conversion lanthanide NPs, in which the AuNCs were engineered with dual ligands for conferring GSH-activated turn on of NIR-II PL (Fig. 6b) [77]. The platform was designed for tumor-associated GSH imaging and synergistic chemo-/photodynamic therapy, showing an effective tumor theranostic strategy.

Based on the fact that surface ligands can seriously affect the PL of AuNCs, Liu et al. presented a ligand exchange strategy for in vivo molecular imaging applications (Fig. 6c) [53]. It was found that TPPTS-protected AuNCs can be sensitively activated by GSH, resulting in the giant enhancement of NIR-II PL intensity. TPPTS-AuNCs were demonstrated for in vivo low-background

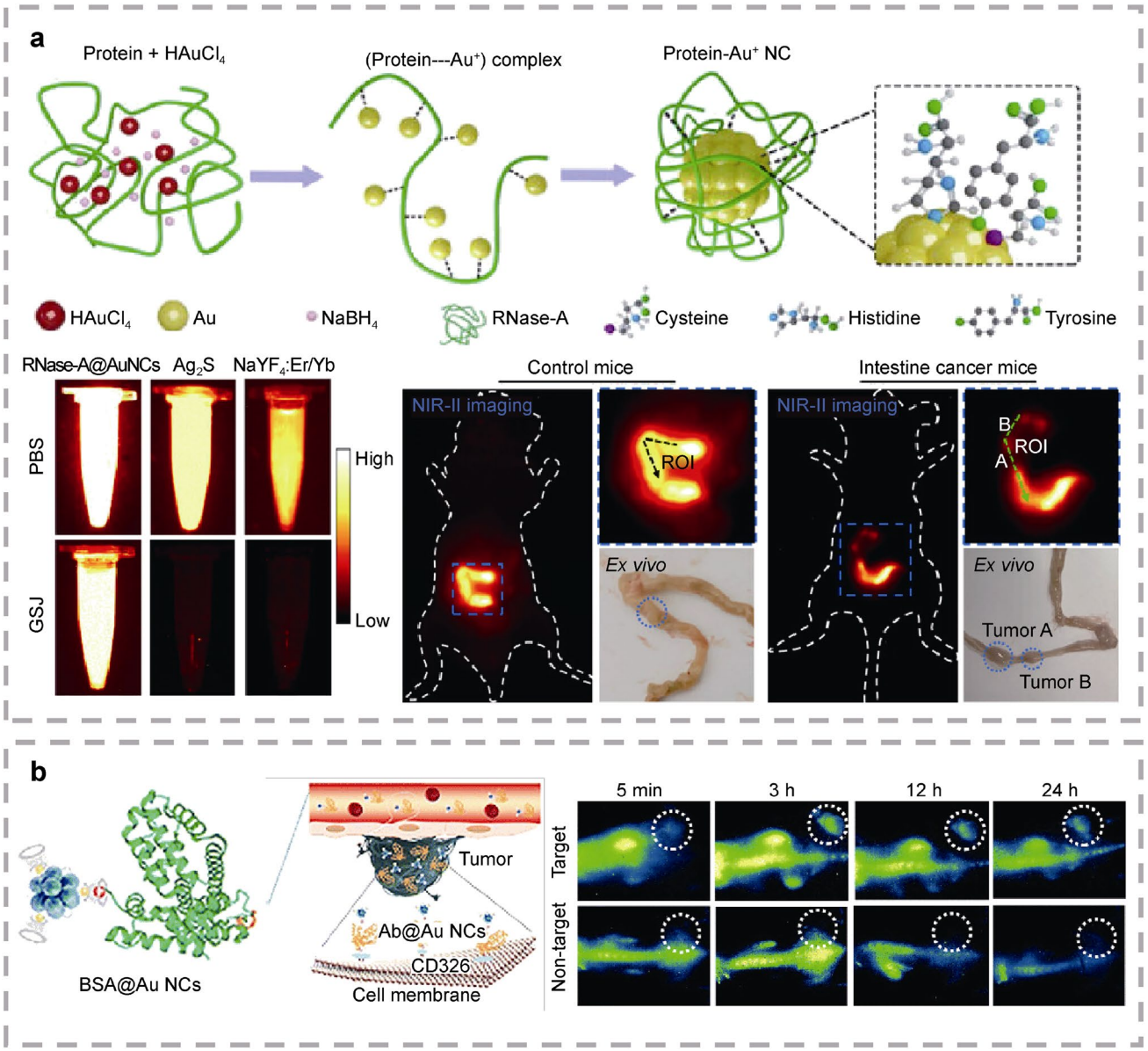

Fig. 4 NIR-II Luminescent AuNCs-based tumor imaging. **a** Schematic representation of the synthesis of RNase-A@AuNCs, and the comparison of their NIR-II PL stability with Ag_2S quantum dots and $NaYF_4$:Er/Yb NPs in simulated gastric juice (SGJ) and PBS. Sensitive NIR-II PL imaging of intestinal tumors was achieved by using the AuNCs. Reproduced with permission from Ref. [42]. Copyright 2020, Wiley–VCH. **b** Schematic diagram of tumor-targeted NIR-II PL imaging based on CDS-AuNCs that enabled the labeling of antibody (Ab) via host–guest interaction. NIR-II PL imaging of mice was shown at various time points post intravenous injection of non-target and target probes, respectively. Reproduced with permission from Ref. [35]. Copyright 2021, Wiley–VCH

imaging of GSH and long-term tracking of acidosis-induced kidney injury. In addition, activatable AuNCs nanoprobes can be designed by coupling with other recognition units and signal generation mechanisms. In a recent study, NIR-II luminescent GSH-AuNCs were embedded in poly-dopamine NPs and further integrated with methylene blue (MB), which quenches the NIR-II PL of AuNCs through the photo-induced electron transfer (PET) effect (Fig. 6d) [78]. Interestingly, MB could be released under acid condition, causing the NIR-II PL turn on of AuNCs. This nanoprobe, thus, enabled the NIR-II PL monitoring of gastric acid secretion in mice and also sensitive diagnosis of gastric ulcer diseases. It is worthy to be mentioned that NIR-II luminescent AuNCs hold great promise for sensitive in vivo molecular imaging with high signal-to-noise ratios as a consequence of their good renal clearance and low nonspecific tissue accumulation capabilities [79–81].

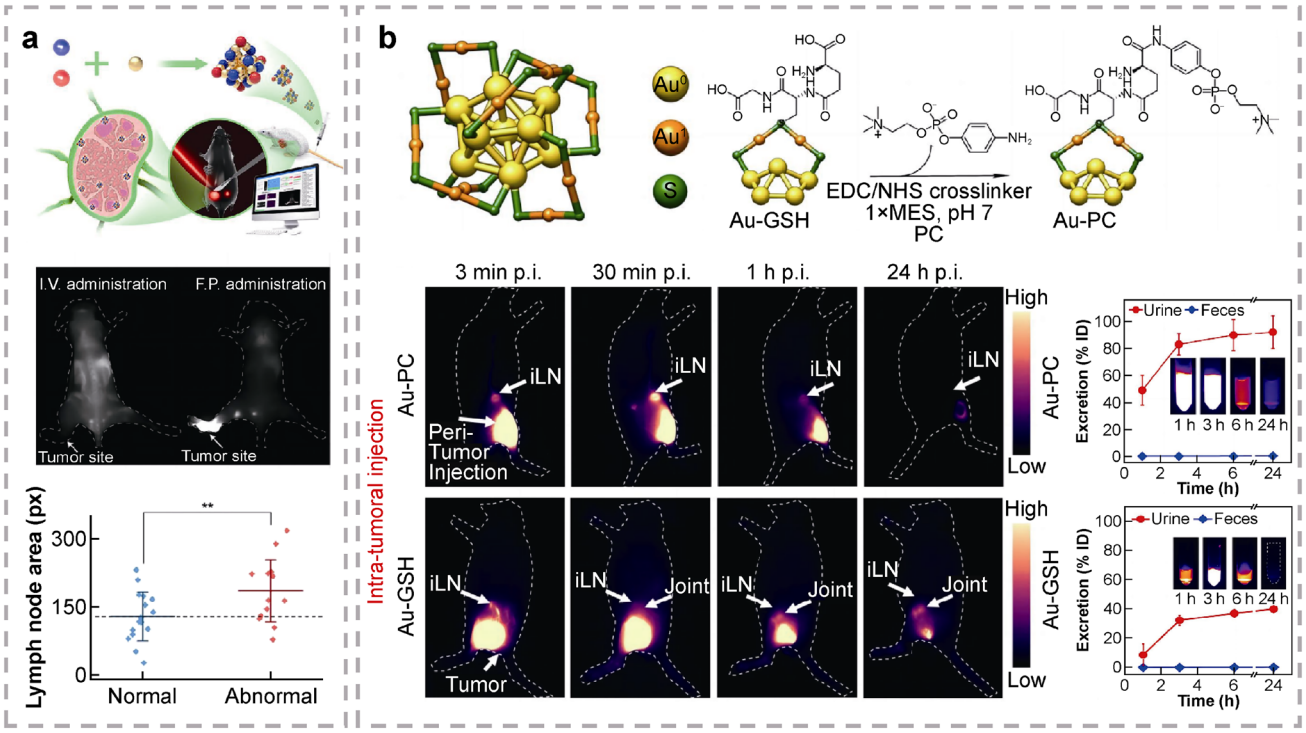

Fig. 5 NIR-II luminescent AuNCs-based tumor metastasis tracking. **a** Schematic of the synthesis and lymph node imaging of AuNCs. In vivo lymph node imaging was performed on tumor-bearing mice, along with showing NIR-II PL distribution areas in the legs of tumor-bearing and normal mice. Reproduced with permission from Ref. [41]. Copyright 2022, American Chemical Society. **b** Lymph node imaging studies based on PC-modified AuNCs. The structure of AuNCs and PC modification were shown. NIR-II PL images of mice were presented after the intratumor injection of AuNCs and PC-AuNCs, respectively. The excretion rates were also determined, revealing the higher renal clearance efficiency of PC-AuNCs than AuNCs. Reproduced with permission from Ref. [68]. Copyright 2022, Springer Nature

4.3 Others

4.3.1 Blood vessel imaging

It is of vital importance to monitor blood vessel structures and blood flow dynamics in disease diagnosis and therapy [82, 83]. For instance, blood vessel injury could cause abnormal blood perfusion and further lead to the damage of brain functions [84, 85]. The sensitive visualization of tumor angiogenesis will help to evaluate tumor invasion and metastasis status [86]. In 2017, Bruns and Bawendi first employed renal clearable AuNCs for in vivo NIR-II PL imaging and enabled higher imaging resolution of mice hindlimb vessels than that of the traditional visible/NIR-I emitting AuNCs (Fig. 7a) [24]. Therewith, Zhang et al. utilized the atomically precise AuNCs for NIR-II PL imaging of the blood vessels in brain and were able to visualize the abnormal blood perfusion in brain injury areas (Fig. 7b) [23]. These works demonstrated the good blood vessel imaging capability of NIR-II luminescent AuNCs. Significantly, Guével and colleagues engineered AuNCs with dithiol pegylated ligands to largely increase NIR-II PL intensity and extend the blood circulation half-life (Fig. 7c) [36]. Such design achieved the high-resolution NIR-II PL imaging of the subtle vascular disorders in mice, as assisted by using a Monte Carlo constrained restoration (MCR) method to process images.

4.3.2 Bone imaging

In vivo bone imaging is a necessary technique to monitor the growth, metabolism, and repair of bone, and also to diagnose bone diseases [88–90]. Currently, there are some fluorescent dyes and NPs for bone imaging, which is generally based on the high affinity of functional phosphate groups to the bone matrix (e.g., hydroxyapatite, HA) [91–93]. In 2020, Cheng and Jia found that GSH-Au_{25}NCs tended to circulate into the bone tissues, except that the majority of AuNCs were eliminated into urine (Fig. 7d) [87]. The AuNCs were demonstrated to bind tightly to HA and further implemented for NIR-II PL imaging of whole-body bony structures. This may provide a new effective strategy for clinical bone imaging in the future.

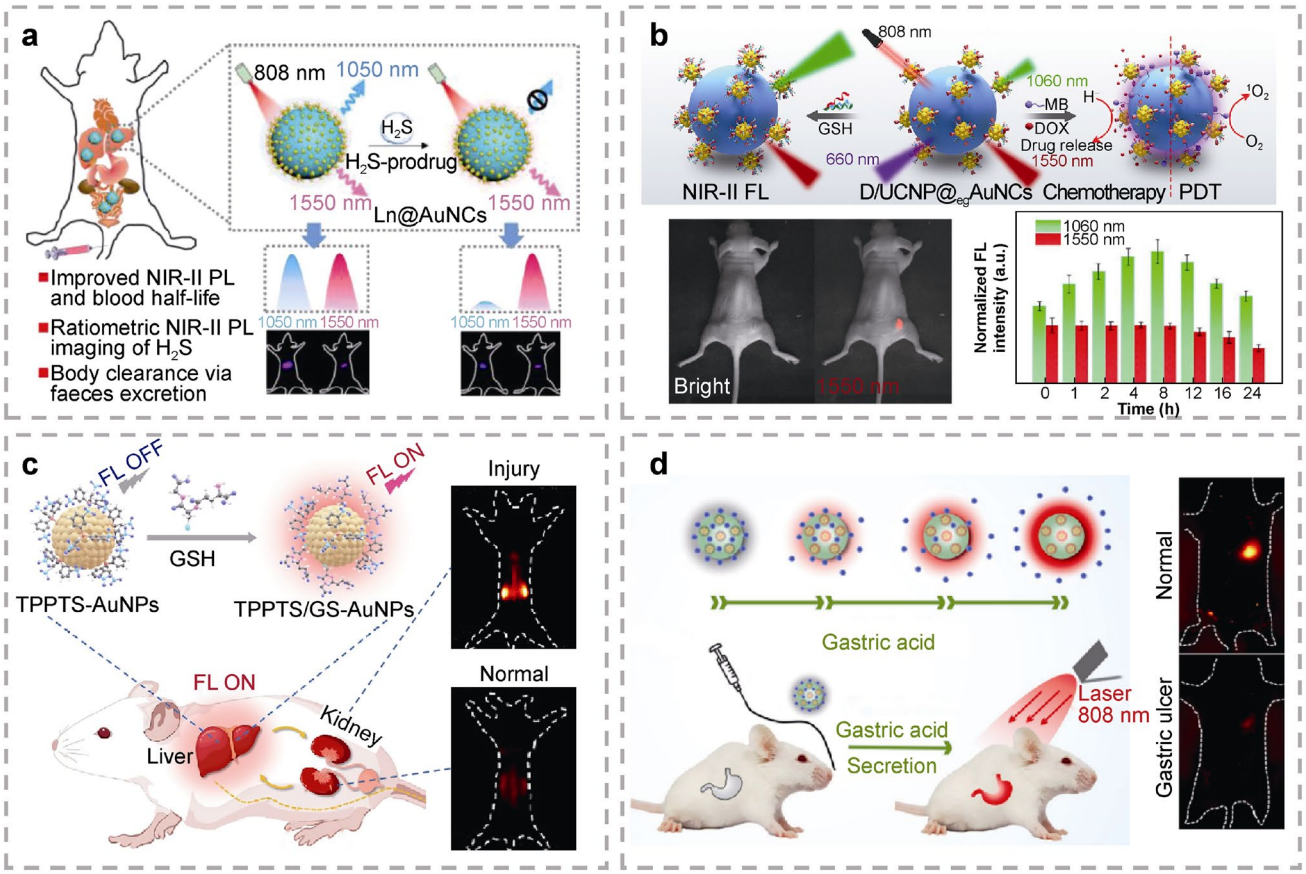

Fig. 6 NIR-II luminescent AuNCs-based molecular imaging applications. **a** Schematic illustration of the ratiometric NIR-II PL imaging of H_2S based on AuNCs-coated lanthanide NPs assemblies. Reproduced with permission from Ref. [34]. Copyright 2022, American Chemical Society; **b** Schematic illustration of the assemblies of AuNCs and lanthanide NPs and their in vivo NIR-II PL imaging of mice tumors. Reproduced with permission from Ref. [77]. Copyright 2023, American Chemical Society; **c** Schematic illustration of in vivo GSH imaging of AuNCs based on the ligand exchange strategy, which enabled early imaging of metabolic acidosis-induced kidney injury. Reproduced with permission from Ref. [53]. Copyright 2023, American Chemical Society; **d** Schematic diagram of the synthesis of poly-dopamine-coated AuNCs (with loading of MB) for in vivo NIR-II PL imaging of gastric acid secretion. Reproduced with permission from Ref. [78]. Copyright 2022, Elsevier

5 Conclusion

In summary, we have comprehensively summarized and discussed recent progress in the synthesis, PL tuning strategies, and bioimaging applications of NIR-II luminescent AuNCs. With the development of optical characterization methods, the fantastic NIR-II PL properties of AuNCs are increasingly discovered, accompanied by their emerging in vivo bioapplications. The review details the fundamental NIR-II PL origins and emission tuning strategies of AuNCs, which have realized the precise synthesis of NIR-II luminescent AuNCs with quantum yields of about 1% (sometimes exceeding 5%). Due to the rapid renal clearance and low nonspecific liver accumulation, AuNCs generally show high signal-to-noise ratios in diverse NIR-II PL bioimaging studies. We have also summarized the design principles and NIR-II PL imaging performance of AuNCs-based nanoprobes. It is believed that the exploration of AuNCs as NIR-II nanoprobes could overcome some challenges faced by other large-size luminescent NPs, thus enabling better imaging specificity and higher clinical translation potential. Therefore, NIR-II luminescent AuNCs are anticipated to offer new powerful tools for the diagnosis and treatment of diverse diseases.

In spite of such developments, the research on NIR-II luminescent AuNCs is still on its infancy. Noteworthy, there remains some challenges to the rational engineering of the NIR-II luminescent AuNCs for in vivo bioimaging and future clinical translation. First, it is a big challenge to keep hydrophilic AuNCs with atomically precise structures in the biological environment. Although it is generally achievable to obtain atomically precise AuNCs in certain reaction conditions, their stability in complex environment, especially in the living organism, is unclear, which also needs more valid characterization methods. Second, the

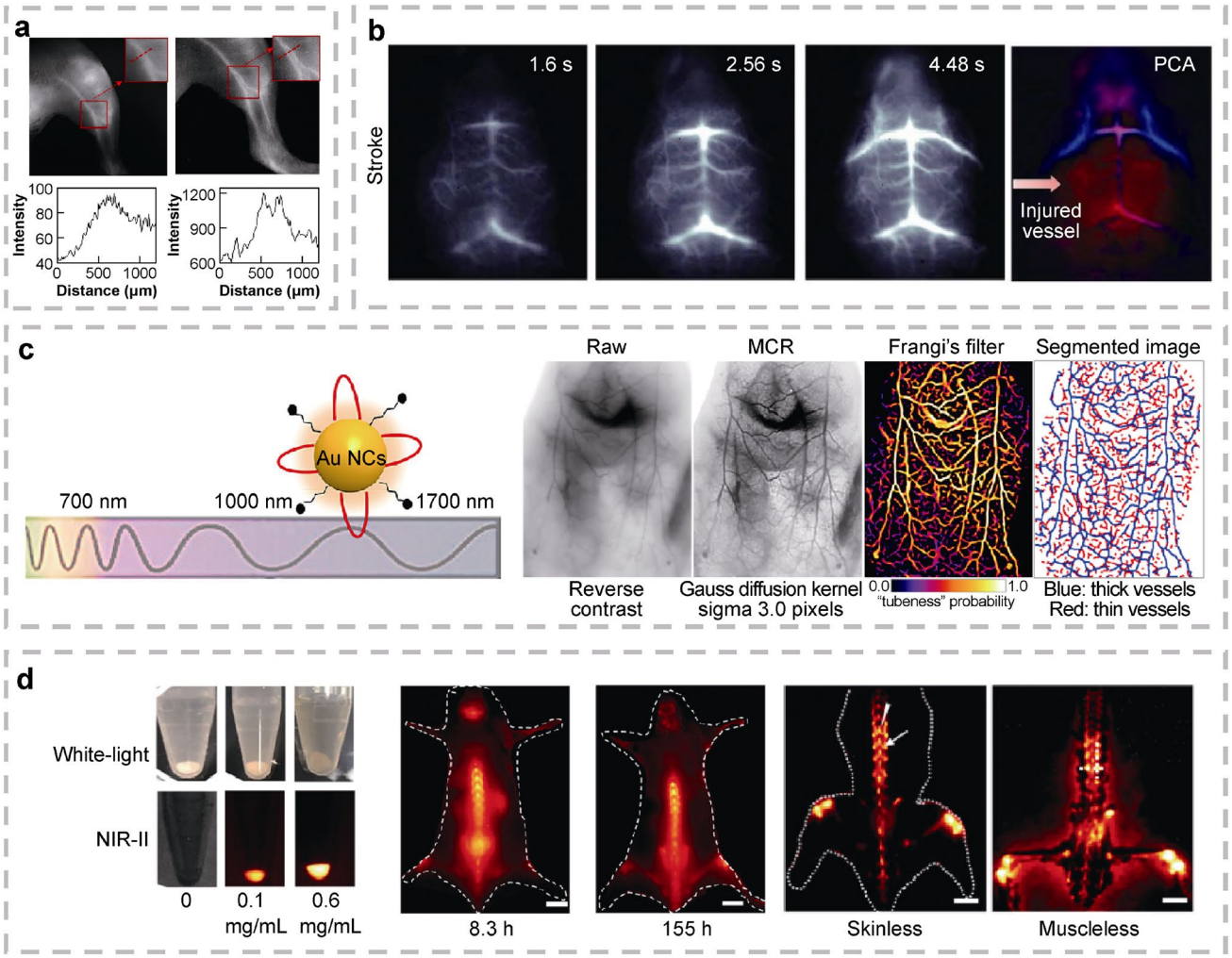

Fig. 7 NIR-II luminescent AuNCs-based blood vessel imaging and bone imaging. **a** NIR-II PL imaging of mice legs after injecting AuNCs with the use of 850-nm LP filter (left) and a 1250-LP filter (right), respectively. Reproduced with permission from Ref. [24]. Copyright 2017, American Chemical Society; **b** Dynamic brain imaging of stroke mouse and PCA overlaid images with arterial (red) and venous (blue) vessels. Reproduced with permission from Ref. [23]. Copyright 2019, Wiley–VCH; **c** Scheme of the MHA/TDT-Au NCs and NIR-II PL images of a Bmp9-KO mouse after MCR processing. Reproduced with permission from Ref. [36]. Copyright 2020, American Chemical Society; **d** White-light images and NIR-II PL images of the precipitates of HA and different concentrations of AuNCs. NIR-II PL images of mice revealed the sensitive bone imaging capability of AuNCs. Reproduced with permission from Ref. [87]. Copyright 2020, Wiley–VCH

NIR-II PL quantum yields of AuNCs are relatively low (e.g., < 5%), which are far lower than other luminescent NPs such as quantum dots and lanthanide NPs. So far, atom doping and ligand engineering strategies are frequently utilized; however, it needs to further enhance quantum yields to enable more sensitive molecular imaging in vivo. Third, it currently seems hard to tune the NIR-II PL wavelength of AuNCs and most of them emitted at around 1100 nm. This hinders the multiple labeling of AuNCs on molecules/cells/tissues for multiplex NIR-II PL imaging. Therefore, it is desired to develop new potent strategies to construct NIR-II PL-tunable AuNCs. Fourth, in vivo targeting efficacy of AuNCs should be further improved, along with clearly unraveling the in vivo transport, biotransformation, and toxicity behaviors. These aspects are the prerequisite for their clinical translation.

Nevertheless, past few years have witnessed the exciting advances of AuNCs in the NIR-II PL bioimaging application. It is believed that NIR-II luminescent AuNCs could provide biocompatible and multifunctional nanoprobes to meet diverse bioapplication scenarios in vivo. With the deepening understandings of materials synthesis, optical tuning and nanoprobe design, NIR-II luminescent AuNCs will show more power in the biomedical fields.

Acknowledgements This work was supported by the National Key Research & Development Program of China (2020YFA0709900), the National Natural Science Foundation of China (22027805, 22274024), the Major Project of Science and Technology of Fujian Province (2020HZ06006), the Young Elite Scientist Sponsorship Program by CAST (YESS20200110), and China Postdoctoral Science Foundation (2022M720737, 2021T140117).

Data availability The data are available from the corresponding authors on reasonable request.

Declarations

Conflict of Interest The authors declare no conflict of interest.

References

1. Tao Y, Li MQ, Ren JS, Qu XG. Metal nanoclusters: novel probes for diagnostic and therapeutic applications. Chem Soc Rev. 2015;44(23):8636–63.
2. Lin ZK, Goswami N, Xue TT, Chai OJH, Xu HJ, Liu YX, Su Y, Xie JP. Engineering metal nanoclusters for targeted therapeutics: from targeting strategies to therapeutic applications. Adv Funct Mater. 2021;31(51):19.
3. Fan Y, Liu SG, Yi Y, Rong HP, Zhang JT. Catalytic nanomaterials toward atomic levels for biomedical applications: from metal clusters to single-atom catalysts. ACS Nano. 2021;15(2):2005–37.
4. Srinivasulu YG, Yao QF, Goswami N, Xie JP. Interfacial engineering of gold nanoclusters for biomedical applications. Mater Horizons. 2020;7(10):2596–618.
5. Yang G, Wang Z, Du F, Jiang F, Yuan X, Ying JY. Ultrasmall coinage metal nanoclusters as promising theranostic probes for biomedical applications. J Am Chem Soc. 2023;145(22):11879–98.
6. Yao Q, Wu Z, Liu Z, Lin Y, Yuan X, Xie J. Molecular reactivity of thiolate-protected noble metal nanoclusters: synthesis, self-assembly, and applications. Chem Sci. 2021;12(1):99–127.
7. Navarro M. Gold complexes as potential anti-parasitic agents. Coord Chem Rev. 2009;253(11–12):1619–26.
8. Tiekink ERT. Gold compounds in medicine: potential anti-tumour agents. Gold Bull. 2003;36(4):117–24.
9. Shaw CF. Gold-based therapeutic agents. Chem Rev. 1999;99(9):2589–600.
10. Hickey JL, Ruhayel RA, Barnard PJ, Baker MV, Berners-Price SJ, Filipovska A. Mitochondria-targeted chemotherapeutics: the rational design of gold(I) N-heterocyclic carbene complexes that are selectively toxic to cancer cells and target protein selenols in preference to Thiols. J Am Chem Soc. 2008;130(38):12570–1.
11. Rigobello MP, Messori L, Marcon G, AgostinaCinellu M, Bragadin M, Folda A, Scutari G, Bindoli A. Gold complexes inhibit mitochondrial thioredoxin reductase: consequences on mitochondrial functions. J Inorg Biochem. 2004;98(10):1634–41.
12. McKeage MJ, Berners-Price SJ, Galettis P, Bowen RJ, Brouwer W, Ding L, Zhuang L, Baguley BC. Role of lipophilicity in determining cellular uptake and antitumour activity of gold phosphine complexes. Cancer Chemother Pharmacol. 2000;46(5):343–50.
13. Sanchez-Delgado RA, Anzellotti A. Metal complexes as chemotherapeutic agents against tropical diseases: trypanosomiasis, malaria and leishmaniasis. Mini Rev Med Chem. 2004;4(1):23–30.
14. Takano S, Tsukuda T. Chemically modified gold/silver superatoms as artificial elements at nanoscale: design principles and synthesis challenges. J Am Chem Soc. 2021;143(4):1683–98.
15. Kang X, Zhu MZ. Tailoring the photoluminescence of atomically precise nanoclusters. Chem Soc Rev. 2019;48(8):2422–57.
16. Yao QF, Yuan X, Chen TK, Leong DT, Xie JP. Engineering functional metal materials at the atomic level. Adv Mater. 2018;30(47):23.
17. Qian HF, Zhu MZ, Wu ZK, Jin RC. Quantum sized gold nanoclusters with atomic precision. Acc Chem Res. 2012;45(9):1470–9.
18. Zheng K, Xie J. Engineering ultrasmall metal nanoclusters as promising theranostic agents. Trends Chem. 2020;2(7):665–79.
19. Zhang L, Wang E. Metal nanoclusters: new fluorescent probes for sensors and bioimaging. Nano Today. 2014;9(1):132–57.
20. Li S, Wei J, Yao Q, Song X, Xie J, Yang H. Emerging ultrasmall luminescent nanoprobes for in vivo bioimaging. Chem Soc Rev. 2023;52(5):1672–96.
21. Porret E, Le Guével X, Coll J-L. Gold nanoclusters for biomedical applications: toward in vivo studies. J Mater Chem B. 2020;8(11):2216–32.
22. Qian S, Wang Z, Zuo Z, Wang X, Wang Q, Yuan X. Engineering luminescent metal nanoclusters for sensing applications. Coord Chem Rev. 2022;451:214268.
23. Liu HL, Hong GS, Luo ZT, Chen JC, Chang JL, Gong M, He H, Yang J, Yuan X, Li LL, Mu XY, Wang JY, Mi WB, Luo J, Xie JP, Zhang XD. Atomic-precision gold clusters for NIR-II imaging. Adv Mater. 2019;31(46):9.
24. Chen Y, Montana DM, Wei H, Cordero JM, Schneider M, Le Guevel X, Chen O, Bruns OT, Bawendi MG. Shortwave infrared in vivo imaging with gold nanoclusters. Nano Lett. 2017;17(10):6330–4.
25. Luo ZT, Yuan X, Yu Y, Zhang QB, Leong DT, Lee JY, Xie JP. From aggregation-induced emission of Au(I)-thiolate complexes to ultrabright Au(0)@Au(I)-thiolate core-shell nanoclusters. J Am Chem Soc. 2012;134(40):16662–70.
26. Zhou C, Long M, Qin Y, Sun X, Zheng J. Luminescent gold nanoparticles with efficient renal clearance. Angew Chem Int Ed. 2011;50(14):3168–72.
27. Xie J, Zheng Y, Ying JY. Protein-directed synthesis of highly fluorescent gold nanoclusters. J Am Chem Soc. 2009;131(3):888–9.
28. Edwards PP, Thomas JM. Gold in a metallic divided state—from faraday to present-day nanoscience. Angew Chem Int Ed. 2007;46(29):5480–6.
29. Negishi Y, Nobusada K, Tsukuda T. Glutathione-protected gold clusters revisited: bridging the gap between Gold(I)−thiolate complexes and thiolate-protected gold nanocrystals. J Am Chem Soc. 2005;127(14):5261–70.
30. Brust M, Walker M, Bethell D, Schiffrin DJ, Whyman R. Synthesis of thiol-derivatised gold nanoparticles in a two-phase Liquid-Liquid system. J Chem Soc Chem Commun. 1994;0(7):801–2.
31. Zhang K, Chen FR, Wang L, Hu J. Second Near-Infrared (NIR-II) Window for Imaging-Navigated Modulation of Brain Structure and Function. Small. 2023;19(14):2206044.
32. Xin Q, Ma H, Wang H, Zhang XD. Tracking tumor heterogeneity and progression with near-infrared II fluorophores. Exploration. 2023;3(2):20220011.
33. Ma H, Wang J, Zhang X. Near-infrared II emissive metal clusters: from atom physics to biomedicine. Coord Chem Rev. 2021;448:214184.
34. Li SH, Ma QP, Wang CL, Yang KD, Hong ZZ, Chen QS, Song JB, Song XR, Yang HH. Near-infrared II gold nanocluster assemblies with improved luminescence and biofate for in vivo ratiometric imaging of H_2S. Anal Chem. 2022;94(5):2641–7.
35. Song XR, Zhu W, Ge XG, Li RF, Li SH, Chen X, Song JB, Xie JP, Chen XY, Yang HH. A new class of NIR-II gold nanocluster-based protein biolabels for in vivo tumor-targeted imaging. Angew Chem Int Ed. 2021;60(3):1306–12.
36. Yu ZX, Musnier B, Wegner KD, Henry M, Chovelon B, Desroches-Castan A, Fertin A, Resch-Genger U, Bailly S, Coll JL,

Usson Y, Josserand V, Le Guevel X. High-resolution shortwave infrared imaging of vascular disorders using gold nanoclusters. ACS Nano. 2020;14(4):4973–81.
37. Yu M, Xu J, Zheng J. Renal clearable luminescent gold nanoparticles: from the bench to the clinic. Angew Chem Int Ed. 2019;58(13):4112–28.
38. Zhang X, Wu D, Shen X, Liu P, Fan F, Fan S. In vivo renal clearance, biodistribution, toxicity of gold nanoclusters. Biomaterials. 2012;33(18):4628–38.
39. Yu Y, Luo Z, Yu Y, Lee JY, Xie J. Observation of cluster size growth in CO-directed synthesis of $Au_{25}(SR)_{18}$ nanoclusters. ACS Nano. 2012;6(9):7920–7.
40. Yang G, Mu X, Pan X, Tang Y, Yao Q, Wang Y, Jiang F, Du F, Xie J, Zhou X, Yuan X. Ligand engineering of Au_{44} nanoclusters for NIR-II luminescent and photoacoustic imaging-guided cancer photothermal therapy. Chem Sci. 2023;14(16):4308–18.
41. Pang ZY, Yan WX, Yang J, Li QZ, Guo Y, Zhou DJ, Jiang XY. Multifunctional gold nanoclusters for effective targeting, near-infrared fluorescence imaging, diagnosis, and treatment of cancer lymphatic metastasis. ACS Nano. 2022;16(10):16019–37.
42. Wang WL, Kong YF, Jiang J, Xie QQ, Huang Y, Li GN, Wu D, Zheng HZ, Gao M, Xu SJ, Pan YX, Li W, Ma RL, Wu MX, Li XH, Zuilhof H, Cai XM, Li RB. Engineering the protein corona structure on gold nanoclusters enables red-shifted emissions in the second near-infrared window for gastrointestinal imaging. Angew Chem Int Ed. 2020;59(50):22431–5.
43. Zhao H, Wang H, Li HR, Zhang TC, Zhang J, Guo WH, Fu K, Du GQ. Magnetic and near-infrared-II fluorescence Au-Gd nanoclusters for imaging-guided sensitization of tumor radiotherapy. Nanoscale Adv. 2022;4(7):1815–26.
44. Dan Q, Yuan Z, Zheng S, Ma HR, Luo WX, Zhang L, Su N, Hu DH, Sheng ZH, Li YJ. Gold nanoclusters-based NIR-II photosensitizers with catalase-like activity for boosted photodynamic therapy. Pharmaceutics. 2022;14(8):17.
45. Tang L, Zeng XD, Zhou H, Gui CH, Luo QL, Zhou WY, Wu J, Li QQ, Li Y, Xiao YL. Theranostic gold nanoclusters for NIR-II imaging and photodynamic therapy. Chem Res Chin Univ. 2021;37(4):934–42.
46. Wang J, Wang ZY, Li SJ, Zang SQ, Mak TCW. Carboranealkynyl-protected gold nanoclusters: size conversion and UV/Vis–NIR optical properties. Angew Chem Int Ed. 2021;133(11):6024–9.
47. Wang G, Huang T, Murray RW, Menard L, Nuzzo RG. Near-IR luminescence of monolayer-protected metal clusters. J Am Chem Soc. 2005;127(3):812–3.
48. Li Q, Zeman CJ, Ma ZR, Schatz GC, Gu XW. Bright NIR-II photoluminescence in rod-shaped icosahedral gold nanoclusters. Small. 2021;17(11):7.
49. Zhou M, Song YB. Origins of visible and near-infrared emissions in $[Au_{25}(SR)_{18}]^-$ nanoclusters. J Phys Chem Lett. 2021;12(5):1514–9.
50. Pyo K, Thanthirige VD, Kwak K, Pandurangan P, Ramakrishna G, Lee D. Ultrabright luminescence from gold nanoclusters: rigidifying the Au(I)-thiolate shell. J Am Chem Soc. 2015;137(25):8244–50.
51. Wang SX, Meng XM, Das A, Li T, Song YB, Cao TT, Zhu XY, Zhu MZ, Jin RC. A 200-fold quantum yield boost in the photoluminescence of silver-doped Ag_xAu_{25-x} nanoclusters: the 13th silver atom matters. Angew Chem Int Ed. 2014;53(9):2376–80.
52. Huang Y, Chen K, Liu L, Ma HZ, Zhang XN, Tan KX, Li Y, Liu Y, Liu CL, Wang H, Zhang XD. Single atom-engineered NIR-II gold clusters with ultrahigh brightness and stability for acute kidney injury. Small. 2023. https://doi.org/10.1002/smll.202300145.
53. Zhao ZP, Chen HR, He K, Lin JC, Cai W, Sun YD, Liu JB. Glutathione-activated emission of ultrasmall gold nanoparticles in the second near-infrared window for imaging of early kidney injury. Anal Chem. 2023;95(11):5061–8.
54. Haye L, Diriwari PI, Alhalabi A, Gallavardin T, Combes A, Klymchenko AS, Hildebrandt N, Le Guével X, Reisch A. Enhancing near infrared II emission of gold nanoclusters via encapsulation in small polymer nanoparticles. Adv Opt Mater. 2022. https://doi.org/10.1002/adom.202201474.
55. Bertorelle F, Wegner KD, Bakulic MP, Fakhouri H, Comby-Zerbino C, Sagar A, Bernado P, Resch-Genger U, Bonacic-Koutecky V, Le Guevel X, Antoine R. Tailoring the NIR-II photoluminescence of single thiolated Au_{25} nanoclusters by selective binding to proteins. Chem-Eur J. 2022;28(39):8.
56. Wen Y, Long ZQ, Huo FJ, Yin CX. Novel strategy for accurate tumor labeling: endogenous metabolic imaging through metabolic probes. Sci China Chem. 2022;65(12):2517–27.
57. Crosby D, Bhatia S, Brindle KM, Coussens LM, Dive C, Emberton M, Esener S, Fitzgerald RC, Gambhir SS, Kuhn P, Rebbeck TR, Balasubramanian S. Early detection of cancer. Science. 2022;375(6586):eaay9040.
58. Hong B, Zu Y. Detecting circulating tumor cells: current challenges and new trends. Theranostics. 2013;3(6):377–94.
59. Zhu H, Fan JL, Du JJ, Peng XJ. Fluorescent probes for sensing and imaging within specific cellular organelles. Acc Chem Res. 2016;49(10):2115–26.
60. Weissleder R, Schwaiger MC, Gambhir SS, Hricak H. Imaging approaches to optimize molecular therapies. Sci Transl Med. 2016;8(355):7.
61. Ueno T, Nagano T. Fluorescent probes for sensing and imaging. Nat Methods. 2011;8(8):642–5.
62. Li YL, Hung WC. Reprogramming of sentinel lymph node microenvironment during tumor metastasis. J Biomed Sci. 2022;29(1):1–15.
63. Heerdt AS. Lymphatic mapping and sentinel lymph node biopsy for breast cancer. JAMA Oncol. 2018;4(3):431.
64. Lee WC, Kopetz S, Wistuba II, Zhang J. Metastasis of cancer: when and how? Ann Oncol. 2017;28(9):2045–7.
65. Chaffer CL, Weinberg RA. A perspective on cancer cell metastasis. Science. 2011;331(6024):1559–64.
66. Tian R, Ma HL, Zhu SJ, Lau J, Ma R, Liu YJ, Lin LS, Chandra S, Wang S, Zhu XF, Deng HZ, Niu G, Zhang MX, Antaris AL, Hettie KS, Yang B, Liang YY, Chen XY. Multiplexed NIR-II probes for lymph node-invaded cancer detection and imaging-guided surgery. Adv Mater. 2020;32(11):10.
67. Li CY, Torres VC, Tichauer KM. Noninvasive detection of cancer spread to lymph nodes: A review of molecular imaging principles and protocols. J Surg Oncol. 2018;118(2):301–14.
68. Baghdasaryan A, Wang F, Ren F, Ma Z, Li J, Zhou X, Grigoryan L, Xu C, Dai H. Phosphorylcholine-conjugated gold-molecular clusters improve signal for Lymph Node NIR-II fluorescence imaging in preclinical cancer models. Nat Commun. 2022;13(1):5613.
69. Zhou ZX, Lu ZR. Molecular imaging of the tumor microenvironment. Adv Drug Deliv Rev. 2017;113:24–48.
70. Chen LY, Wang CW, Yuan ZQ, Chang HT. Fluorescent gold nanoclusters: recent advances in sensing and imaging. Anal Chem. 2015;87(1):216–29.
71. Chen LL, Lyu Y, Zhang X, Zheng LT, Li QQ, Ding D, Chen FM, Liu YH, Li W, Zhang YT, Huang QL, Wang ZQ, Xie TT, Zhang Q, Sima Y, Li K, Xu S, Ren TB, Xiong MY, Wu Y, Song JB, Yuan L, Yang HH, Zhang XB, Tan WH. Molecular imaging: design mechanism and bioapplications. Sci China Chem. 2023. https://doi.org/10.1007/s11426-022-1461-3.
72. Fang H, Yu H, Lu Q, Fang X, Zhang Q, Zhang J, Zhu L, Ma Q. A new ratiometric fluorescent probe for specific monitoring of

hROS under physiological conditions using boric acid-protected L-DOPA gold nanoclusters. Anal Chem. 2020;92(19):12825–32.
73. Ju E, Liu Z, Du Y, Tao Y, Ren J, Qu X. Heterogeneous assembled nanocomplexes for ratiometric detection of highly reactive oxygen species in vitro and in vivo. ACS Nano. 2014;8(6):6014–23.
74. Bai XL, Xu SY, Wang LY. Full-range pH stable Au-clusters in nanogel for confinement-enhanced emission and improved sulfide sensing in living cells. Anal Chem. 2018;90(5):3270–5.
75. Xiang H, He SY, Zhao G, Zhang MT, Lin J, Yang LN, Liu HL. Gold nanocluster-based ratiometric probe with surface structure regulation-triggered sensing of hydrogen sulfide in living organisms. ACS Appl Mater Interfaces. 2023;15(10):12643–52.
76. Chen TT, Hu YH, Cen Y, Chu X, Lu Y. A dual-emission fluorescent nanocomplex of gold-cluster-decorated silica particles for live cell imaging of highly reactive oxygen species. J Am Chem Soc. 2013;135(31):11595–602.
77. Hu SQ, Huang LX, Zhou LY, Wu TC, Zhao SL, Zhang LL. Single-excitation triple-emission down-/up-conversion nanoassemblies for tumor microenvironment-enhanced ratiometric NIR-II fluorescence imaging and chemo-/photodynamic combination therapy. Anal Chem. 2023;95(7):3830–9.
78. Liang M, Hu Q, Yi SX, Chi YJ, Xiao Y. Development of an Au nanoclusters based activatable nanoprobe for NIR-II fluorescence imaging of gastric acid. Biosens Bioelectron. 2023;224:9.
79. Yang J, Wang T, Zhao LN, Rajasekhar VK, Joshi S, Andreou C, Pal S, Hsu HT, Zhang HW, Cohen IJ, Huang RM, Hendrickson RC, Miele MM, Pei WB, Brendel MB, Healey JH, Chiosis G, Kircher MF. Gold/alpha-lactalbumin nanoprobes for the imaging and treatment of breast cancer. Nat Biomed Eng. 2020;4(7):686–703.
80. Loynachan CN, Soleimany AP, Dudani JS, Lin YY, Najer A, Bekdemir A, Chen Q, Bhatia SN, Stevens MM. Renal clearable catalytic gold nanoclusters for in vivo disease monitoring. Nat Nanotechnol. 2019;14(9):883–90.
81. Jiang XY, Du BJ, Zheng J. Glutathione-mediated biotransformation in the liver modulates nanoparticle transport. Nat Nanotechnol. 2019;14(9):874–82.
82. de Palma M, Biziato D, Petrova TV. Microenvironmental regulation of tumour angiogenesis. Nat Rev Cancer. 2017;17(8):457–74.
83. Tu CY, Das S, Baker AB, Zoldan J, Suggs LJ. Nanoscale strategies: treatment for peripheral vascular disease and critical limb ischemia. ACS Nano. 2015;9(4):3436–52.
84. Yang Y, Rosenberg GA. Blood-brain barrier breakdown in acute and chronic cerebrovascular disease. Stroke. 2011;42(11):3323–8.
85. Rosell A, Cuadrado E, Ortega-Aznar A, Hernandez-Guillamon M, Lo EH, Montaner J. MMP-9-Positive neutrophil infiltration is associated to blood-brain barrier breakdown and basal lamina type IV collagen degradation during hemorrhagic transformation after human ischemic stroke. Stroke. 2008;39(4):1121–6.
86. Viallard C, Larrivee B. Tumor angiogenesis and vascular normalization: alternative therapeutic targets. Angiogenesis. 2017;20(4):409–26.
87. Li DL, Liu Q, Qi QR, Shi H, Hsu EC, Chen WY, Yuan WL, Wu YF, Lin SE, Zeng YT, Xiao ZY, Xu LY, Zhang YR, Stoyanova T, Jia W, Cheng Z. Gold nanoclusters for NIR-II fluorescence imaging of bones. Small. 2020;16(43):9.
88. Zou D, Lin R, Han Y, Jia J, Zhou G, Zhang H, Ge K. Lanthanum promoting bone formation by regulating osteogenesis, osteoclastogenesis and angiogenesis. J Rare Earths. 2023. https://doi.org/10.1016/j.jre.2023.01.019.
89. Wu P, Siegwart DJ, Xiong H. Recent advances in the targeted fluorescent probes for the detection of metastatic bone cancer. Sci China Chem. 2021;64(8):1283–96.
90. Zaheer A, Lenkinski RE, Mahmood A, Jones AG, Cantley LC, Frangioni JV. In vivo near-infrared fluorescence imaging of osteoblastic activity. Nat Biotechnol. 2001;19(12):1148–54.
91. Sun WT, Ge K, Jin Y, Han Y, Zhang HS, Zhou GQ, Yang XJ, Liu DD, Liu HF, Liang XJ, Zhang JC. Bone-targeted nanoplatform combining zoledronate and photothermal therapy to treat breast cancer bone metastasis. ACS Nano. 2019;13(7):7556–67.
92. Xiong H, Zuo H, Yan YF, Occhialini G, Zhou KJ, Wan YH, Siegwart DJ. High-contrast fluorescence detection of metastatic breast cancer including bone and liver micrometastases via size-controlled pH-activatable water-soluble probes. Adv Mater. 2017;29(29):10.
93. Li CY, Zhang YJ, Chen GC, Hu F, Zhao K, Wang QB. Engineered multifunctional nanomedicine for simultaneous stereotactic chemotherapy and inhibited osteolysis in an orthotopic model of bone metastasis. Adv Mater. 2017;29(13):7.